ChemInform Abstract: Covalent Guest–Framework Interactions in Heavy Metal Sodalites: Structure and Properties of Thallium and Silver Sodalite.

ARTICLE · AUGUST 1999

DOI: 10.1021/jp990898i

5 AUTHORS, INCLUDING:

Joseph R. Sachleben
University of Chicago
33 PUBLICATIONS **725** CITATIONS

Covalent Guest−Framework Interactions in Heavy Metal Sodalites: Structure and Properties of Thallium and Silver Sodalite

Susan E. Latturner,[†] Joseph Sachleben,[‡] Bo B. Iversen,[§] Jonathan Hanson,[||] and Galen D. Stucky*[,†,‡]

Department of Chemistry and Materials Research Laboratory, University of California, Santa Barbara, California 93106, Department of Chemistry, University of Aarhus, Denmark DK-8000, and Department of Chemistry, Brookhaven National Laboratory, Upton New York 11973

Received: March 15, 1999; In Final Form: June 19, 1999

Covalent bonds between the heavy metal cations and the aluminosilicate framework have been discovered to be the cause of distinct structural characteristics in anhydrous sodalites $Ag_6[AlSiO_4]_6$ and $Tl_6[AlSiO_4]_6$ that differ significantly from their alkali metal containing analogues. Evidence of guest−framework bonding interactions include interatomic distances, shifted IR bands, and quadrupole coupling of aluminum. This bonding results in a reduction of the unit cell size, and a locked in static disorder of the cations. Also of interest are the short Tl−Tl distances seen in $Tl_6[AlSiO_4]_6$. These could indicate the formation of Tl_3^{3+} species in each cage, resulting in a bcc lattice of ionic thallium clusters. Low-temperature synchrotron powder diffraction data, multiple quantum magic-angle spinning (MQ-MAS) NMR, and FTIR studies are presented.

Introduction

Sodalites are aluminosilicate framework structures with the general composition $M_{6+y}[AlSiO_4]_6(X)_y \cdot nH_2O$. The framework, consisting of alternating, corner sharing SiO_4 and AlO_4 tetrahedra, is a space-filling assembly of β-cages which have the shape of truncated octahedra; see Figure 1. To compensate for the negative charge of the host framework, each cage contains a net positively charged collection of cations (M^+), anions (X^-), and water molecules. The naturally occurring mineral sodalite, $Na_8[AlSiO_4]_6Cl_2$, has a Na_4Cl^{3+} group in each cage.[1] Much work has been done investigating various M_4X^{3+} species in sodalite because of the potential for creating a bcc lattice of confined clusters. Both semiconducting moieties (such as Ag_4Cl^{3+})[2] and metallic clusters (such as $Na_4[e^-]^{3+}$)[3] have been encapsulated in the lattice to determine the interactions of such species when enclosed in an insulating aluminosilicate framework.[4] The electronic properties of these clusters will have a complex dependence on the interactions between the atoms in the cage and their coupling to the framework. These forces will also determine whether the clusters behave as isolated centers or have some degree of wavefunction overlap between the cages. With cations, anions, and possible neutral species present in many sodalites, differentiating between the many potential effects can be difficult. The compounds studied in this paper, $Ag_6[AlSiO_4]_6$ and $Tl_6[AlSiO_4]_6$, contain only the three cations per cage necessary for charge balancing, therefore minimizing the kinds of interactions that can be present.

Depending on the exact nature of the cage-filling species, the sodalite framework can adjust itself by increasing or decreasing the volume of the unit cell. The geometrical distortions connected with such a volume change are generally ascribed to tilting of the TO_4 tetrahedra (T = Al, Si) by cooperative rotations about their −4 axes.[5] This results in bending of the Si−O−Al angle, which varies between 123° and 160.5° (the latter is the theoretical maximum, for tetrahedra with a tilt angle $\langle\varphi\rangle = 0°$). It is generally observed that the T−O bond lengths do not change significantly, remaining near the average values of 1.70 Å for Al−O and 1.65 Å for Si−O bonds. The nature and extent of the distortions are related to the interactions between the framework and the guest ions and between the guest ions themselves. Using the information gleaned from such distortions, a considerable number of zeolite structures have been categorized, predictions about stability made, and phase transition mechanisms understood.[6]

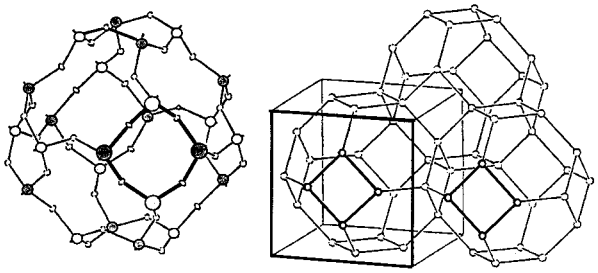

Figure 1. Sodalite beta cage. Oxygens are omitted for clarity from the structure on the right to show the packing of the cages in the structure. Figure modified from ref 21.

In the present investigation, we observe covalent bonding of heavy metal cations to the framework oxygens of sodalite; these bonds appear to have characteristics between those of the strongly linked Bronsted acid sites in catalytic zeolites and the predominantly electrostatic interactions found in alkali metal containing analogues. Dehydrated sodalite, $Na_6[AlSiO_4]_6$, is one of the simplest open-framework aluminosilicate materials, and a good model compound for the many other structures containing β-cage units. The heavy cations Tl^+ and Ag^+ were substituted for Na^+ in this compound, and the effects on the framework were determined using X-ray powder diffraction, ^{27}Al multiple-quantum MAS NMR, and FTIR spectroscopy. The

[†] Department of Chemistry, University of California.
[‡] Materials Research Laboratory, University of California.
[§] University of Aarhus.
[||] Brookhaven National Laboratory.

10.1021/jp990898i CCC: $18.00
Published on Web 08/05/1999

sodium analogue was also studied and is discussed here for comparison.[7] Because of the strong interactions of the heavy metal ions with the framework, it was found that many correlations between IR, NMR, and structural data that have been empirically determined for alkali metal sodalites do not hold for the compounds studied here.

Experimental Section

Synthesis. The starting material $Na_8[AlSiO_4]_6(OH)_2 \cdot 2H_2O$ (hydroxysodalite) was prepared hydrothermally from a basic solution of aluminum isopropoxide and tetraethyl orthosilicate. A 10.213 g amount of aluminum isopropoxide (0.050 mol; Strem chemicals, 99.99%) and 40.0 g NaOH (1.0 mol; Fisher Chemicals, 98.5%) were placed in a Parr bomb Teflon container along with a magnetic stir bar. Water was added, and the mixture was stirred until the solids dissolved. A 10.42 g amount of tetraethyl orthosilicate (0.050 mol; Acros, 98%) was then added dropwise with stirring. After enough water was added to ensure the Teflon vessel was 75% full, it was placed into the steel jacket and the reactants were heated at 180 °C for 10 days. This route was used to avoid incorporation of iron into the product, a common problem for syntheses beginning with Kaolin or alumina. It also provides smaller particle sizes, facilitating faster ion exchange. Soxhlet extraction was used to remove NaOH to convert this product to hydrosodalite, $Na_6[AlSiO_4]_6 \cdot 8H_2O$. The extent of extraction was monitored by powder X-ray diffraction (Scintag PADX diffractometer) and thermogravimetric analysis (Netzsch STA 409 Simultaneous Thermal Analysis system). When the XRD pattern indicated complete conversion to hydrosodalite and there was no weight loss at 700−800 °C in the TGA (indicating loss of any remaining OH^- groups; the water molecules in the cages are removed at 400 °C), the extraction was deemed complete. This compound was used for ion exchange.

Soft, heavy ions such as Ag^+ and Tl^+ exchange very readily into sodalite. Silver exchange has been found to be complete after one exchange cycle in silver nitrate solution at 100 °C.[6c] To ensure complete exchange, two 24 h cycles at 70 °C were used, in 100 mL of 0.7 M $AgNO_3$ for every 1 g of sodalite. Use of a more concentrated solution led to degradation of the crystallinity, indicated by lower intensity and broadening of the X-ray reflections and growth of a broad amorphous signal at 20−30° 2θ. Thallium exchange was carried out in 1 M $TlNO_3$ (100 mL for every 1 g of sodalite) at 100 °C. All manipulations of $TlNO_3$ powders and solutions were done with care as thallium compounds are very toxic. Exchange was complete in four cycles. The extent of exchange was monitored by XRD and elemental analysis using ICP (Thermo Jarrell Ash IRIS HR-ICP spectrometer). The unit cell changed from the 8.885 Å of sodium hydrosodalite to 8.982 Å for silver hydrosodalite and 8.972 Å for thallium hydrosodalite. The water content measured by TGA indicates stoichiometries of $Ag_6[AlSiO_4]_6 \cdot 8H_2O$ and $Tl_6[AlSiO_4]_6 \cdot 8H_2O$. These sodalites were dried at 425 °C for 5 h under a vacuum of 10^{-5} Torr. The thallium sodalite remained white; the dehydrated silver sodalite appeared grayish yellow. This coloration might indicate reduction of some surface silver species, although no ESR signal was observed for the compound. Other samples of $Ag_6[AlSiO_4]_6$ were prepared with less coloration; these had an identical X-ray pattern to the grayish yellow sample studied here. It is therefore unlikely that a small amount of surface reduction has any affect on the overall structure of this sodalite.

X-ray Powder Diffraction. The measurements were carried out at beamline X7B at the National Synchrotron Light Source at Brookhaven National Laboratory. Samples were contained in 0.7 mm quartz capillaries sealed under dry argon to maintain the dehydrated state of the material. 200 × 400 mm Fuji image plates (IPs) were used for intensity recording, and the plates were scanned off line on a Fuji BAS2000 scanner with a pixel size of 0.1 × 0.1 mm. Detailed description of the X7B beamline characteristics and experimental setup for IP powder diffraction measurement have been reported by Norby.[8] Cooling to 100 K was achieved with an OXFORD cryocooler using nitrogen gas flow. The wavelength as well as geometrical parameters for the experimental setup (detector distance, zero point, and IP tilt angle) were determined from refinement of a diffraction pattern taken on a LaB_6 standard sample (NIST #660, $a = 4.15695$ Å). To ensure good signal-to-noise ratios, plates were exposed for 1 h with the temperature fixed at 100 K. For the silver sodalite, a high-resolution 2 h diffraction pattern was also recorded at long wavelength ($\lambda = 1.4879$ Å) with large detector-to-sample distance (365 mm) in order to further resolve possible superstructure reflections, but none were found. To avoid saturation, the IPs were scanned with low sensitivity making sure that the patterns always had a properly recorded background intensity, i.e., no peaks were cut from below.[9] The diffraction patterns were extracted from the IP data by integration over a narrow 50 pixel rectangular strip around the center of the image. The data were corrected for Lorentz, polarization (95% polarized beam), and zero-point effects,[10] and transformed to equivalent step size for use directly in the Rietveld refinement program GSAS.[11] In the Rietveld analysis, each data point was assigned a standard uncertainty based on counting statistics only ($\sigma(I) = \sqrt{I}$). Crystallographic data and further experimental details can be found in the Supporting Information.

Rietveld Analysis. Autoindexing of the diffraction patterns immediately gave solutions based on a cubic crystal system for both heavy metal sodalites. For both patterns, excellent least-squares indexing measures were obtained with all lines being indexed. In contrast to results obtained for $Na_6[AlSiO_4]_6$ (vide infra), no indications of a noncubic crystal system were found. In other words, even with the powerful synchrotron beam, a very sensitive detector, and the low temperature of the experiments, no superstructure reflections were detected for either $Ag_6[AlSiO_4]_6$ or $Tl_6[AlSiO_4]_6$. In both diffraction patterns, a small extraneous line was found at $d = 3.95$ Å that was not observable on the less powerful and lower resolution Scintag diffractometer. The extra line is more prevalent in $Ag_6[AlSiO_4]_6$, where a small line is also observed at $d = 5.5$ Å. The lines are assigned as impurity lines rather than superstructure because exactly the same line is present in both patterns.

For structural refinements, the program GSAS was used. Anomalous scattering contributions at the chosen synchrotron wavelength were included in the refinements, which employed neutral atomic scattering factors. Positional parameters for the M and O atoms were refined together with isotropic thermal parameters on all framework atoms. On the nonframework metal atoms, anisotropic thermal parameters were employed. For both structures, a lower cubic space group (*P*23) was tested in Rietveld refinements. The use of *P*23 has only small effects on the refinement residuals but leads to unrealistic framework geometries. Use of a higher space group (*I*-43*n*) in which the Si and Al atoms are indistinguishable also has negligible effects on the refinements. However, since Lowenstein's rule[12] tends to be strictly observed for zeolites with Al/Si ratios of 1, alternating Al and Si positions are expected, appropriate for the spacegroup *P*-43*n*. In both refinements, pseudo-Voigt profile parameters were used and the backgrounds were modeled with

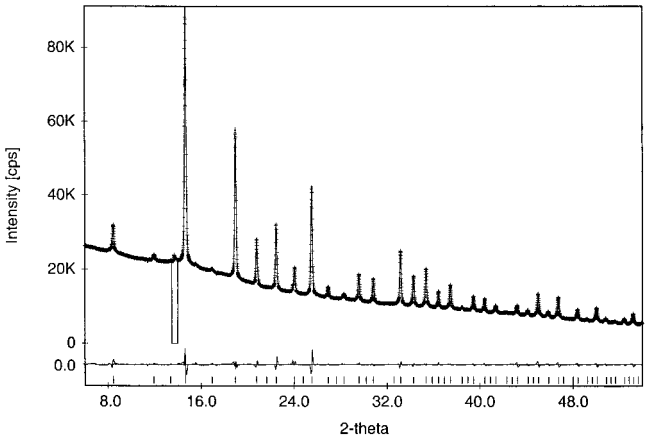

Figure 2. Synchrotron data for $Tl_6[AlSiO_4]_6$ at 100 K.

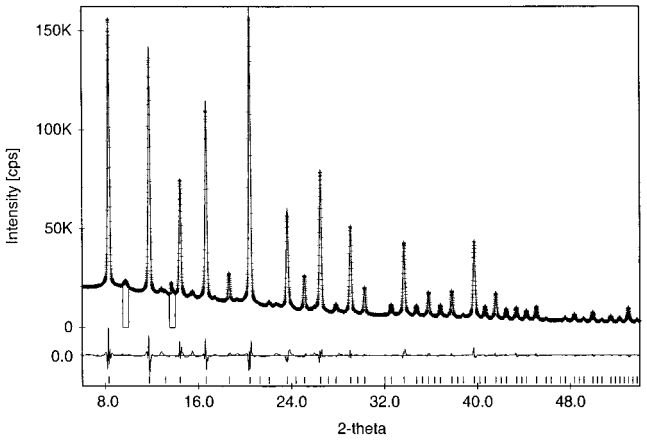

Figure 3. Synchrotron data for $Ag_6[AlSiO_4]_6$ at 100 K.

TABLE 1: Atomic Positions

	occupancy	site	*X*/*a*	*Y*/*b*	*Z*/*c*	*U* (Å^2)[a]
			$Ag_6[AlSiO_4]_6$			
Si	1	6d	1/4	0	1/2	0.018(3)
Al	1	6c	1/4	1/2	0	0.026(4)
O	1	24i	0.1420(8)	0.4602(3)	0.1482(8)	0.025(1)
Ag	0.75	8e	0.2419(1)	0.2419(1)	0.2419(1)	0.0380(4)
						0.0129(4)
			$Tl_6[AlSiO_4]_6$			
Si	1	6d	1/4	0	1/2	0.010(6)
Al	1	6c	1/4	1/2	0	0.044(8)
O	1	24i	0.1474(38)	0.4411(5)	0.1413(38)	0.020(2)
Tl	0.75	8e	0.14723(6)	0.14723(6)	0.14723(6)	0.0286(5)
						0.0028(4)

[a] Anisotropic thermal parameters were used for the heavy metal ions; U_{11} and U_{12} are listed.

Chebyshev polynomia. In final cycles, full-matrix least-squared refinements were carried out with all parameters varied simultaneously. The diffraction patterns, including difference plots from the Rietveld refinement, are shown in Figures 2 and 3. Refinement residuals were $R_{wp} = 0.048$ and $R_F = 0.034$ for $Ag_6[AlSiO_4]_6$ and $R_{wp} = 0.019$ and $R_F = 0.047$ for $Tl_6[AlSiO_4]_6$; further refinement parameters can be found in the Supporting Information. Structural parameters derived from Rietveld analysis are shown in Table 1; bond lengths and bond angles are shown in Table 2. For comparison, the parameters obtained for sodium sodalite at 673 K are also listed.

NMR. The NMR experiments were run on a Bruker AMX 500 spectrometer, using a Doty 5 mm high-speed MAS probe with spinning speeds of 9−10 kHz. ^{27}Al and ^{29}Si magic-angle spinning (MAS) NMR were used to investigate how the sodalite framework is affected by changing the charge balancing cation in the cage. The larmor frequencies for ^{27}Al and ^{29}Si on this spectrometer are 130.3 and 99.4 MHz, respectively.

TABLE 2: Structural Parameters for Dehydrated Sodalites

	$Ag_6[AlSiO_4]_6$	$Tl_6[AlSiO_4]_6$	$Na_6[AlSiO_4]_6$
a (Å)	9.1189(1)	8.9653(1)	9.1603(1)
Si−O (Å)	1.63(1)	1.65(4)	1.605(5)
Al−O (Å)	1.71(1)	1.72(4)	1.709(5)
M−O (Å)	2.3350(3)	2.635(5)	2.569(9)
	2.953(3)	3.225(4)	2.707(7)
M−M (Å)			
intracage	6.240(3)	3.734(2)	6.110(2)
intercage	4.5641(1)	5.1851(8)	4.600(2)
M−(0,0,0) (Å)	3.821(2)	2.2863(9)	3.74(1)
O−Si−O (deg)	108.8(1) (×4)	108.6(4) (×4)	107.3(1) (×4)
	110.8(2) (×2)	111.2(7) (×2)	113.8(2) (×2)
O−Al−O (deg)	109.33(9) (×4)	108.1(4) (×4)	108.1(1) (×4)
	109.8(2) (×2)	112.3(8) (×2)	112.4(2) (×2)
Al−O−Si (deg)	149.0(4)	139.6(3)	155.9(3)
O−M−O (deg)	119.7(2)	91.1(2)	117.2(2)
$\langle\varphi\rangle$	15.0	22.7	9.2

Complications can arise in aluminum NMR because it is a spin 5/2 nucleus and therefore experiences a nuclear quadrupole interaction; this affects the spectrum to second order and produces a broadening and a shift of the NMR resonance even under MAS conditions.[13] Analysis of these quadrupolar effects results in extra information not available with spin-1/2 nuclei. The magnitude of the quadrupole interaction is expressed by the quadrupole coupling constant (QCC), and the geometry of the electric field gradient is described by the asymmetry parameter η, which has 0 value for axial symmetry and approaches a maximum value of 1 as the asymmetry increases. Because they depend on the symmetry of the charge distribution around the nucleus, these parameters can provide a sensitive probe of the local structure and electric field gradients at the aluminum sites of the different sodalites. This quadrupolar broadening can make it difficult to resolve individual chemical environments in the solid; however, in the last 10 years, three very powerful techniques have been developed to circumvent this problem. Double rotation (DOR) and dynamic angle spinning (DAS) were developed in the late 1980s; both involve spinning the sample about two different axes in order to remove the quadrupole effects.[14]

We utilized the more recently developed multiple quantum MAS (MQ-MAS), a procedure which requires spinning only at a single angle and is therefore achievable using a standard MAS probe. This two-dimensional technique correlates a multiple quantum resonance during the first evolution period with the normally observed single quantum transition during acquisition. After 2D Fourier transformation and shearing, an isotropic−anisotropic correlation is produced. The projection onto the isotropic axis is a high-resolution "liquidlike" spectrum that allows the resolution of individual chemical environments in the sample. Slices in the anisotropic dimension give MAS powder pattern line shapes that are sensitive to QCC and η.[15] This technique has been used by several groups on aluminum-containing framework species.[16] It was crucial in distinguishing at least nine different Al sites in AlPO-40, which indicated that its previously assigned space group $P112/n$—which predicts eight aluminum sites—was wrong.[16b] Initial MQ-MAS studies of some of the alkali metal $M_6[AlSiO_4]_6$ analogues reveal several distinct aluminum sites, evidence of distortion and lowered symmetry of the unit cell (vide infra).[7]

The particular technique used in this investigation is the shifted echo pulse sequence described by Grandinetti.[15b] This sequence uses a high-power, nonselective 720° pulse to excite

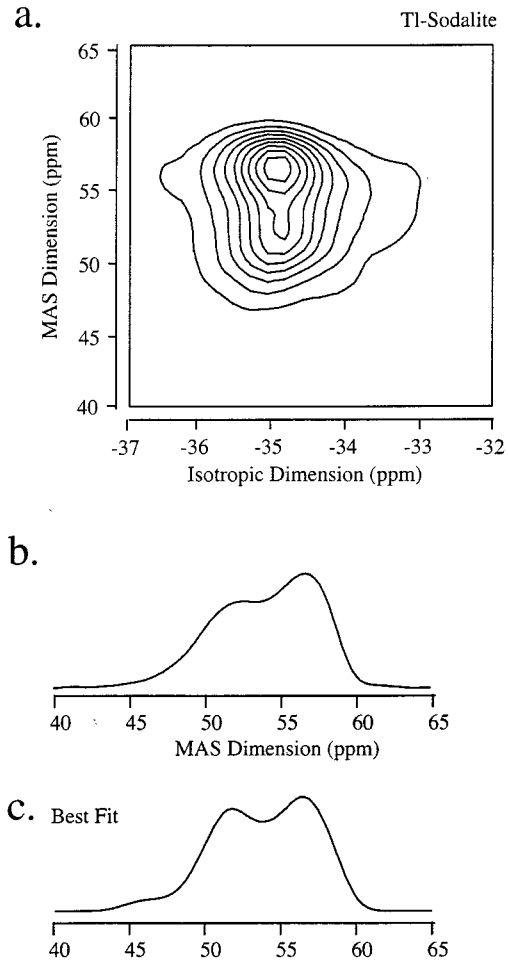

Figure 4. ^{27}Al MQ-MAS NMR data for $Tl_6[AlSiO_4]_6$. Spectrum measured at 130.34 MHz. The quadrupolar splitting is along the ordinate axis, and chemical shift data is along the abscissa. Slices of data along the chemical shift axis are expanded in (b).

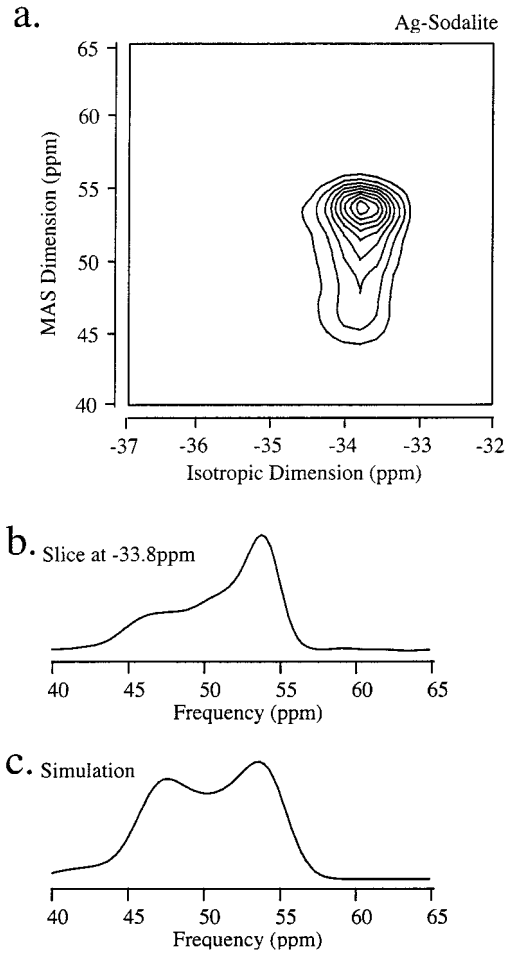

Figure 5. ^{27}Al MQ-MAS NMR data for $Ag_6[AlSiO_4]_6$. Spectrum measured at 130.34 MHz. The quadrupolar splitting is along the ordinate axis, and chemical shift data are along the abscissa. Slices of data along the chemical shift axis are expanded in (b).

and de-excite the triple quantum resonance on ^{27}Al. In our experiments, these pulses were typically 20−25 μs long, which corresponds to rf fields of 80−100 kHz. A soft, low-power 180° pulse (selective for the central transition) is used to refocus the magnetization before acquisition so that probe ringing and receiver dead time problems are avoided. This pulse length was also typically 20−25 μs (rf field strengths of 20−25 kHz). The delay between the pulses was set to an integer multiple of the period of the spinning rate to ensure that a complete, refocused echo signal was obtained. Simulations and fits of the anisotropic slices from the 2D experiments were performed with Phillip Grandinetti's program QUADFIT to determine the values of QCC and η.[17]

The two-dimensional MQMAS spectra and anisotropic slices of the heavy metal sodalites are shown in Figures 4 and 5. For the 2D spectra, the high-resolution isotropic axis is the ordinate and the anisotropic MAS axis is the abscissa. Figures 4b and 5b show 1D anisotropic slices taken at −34.8 ppm and −33.8 ppm in the isotropic dimension for Tl− and Ag−sodalite, respectively. The best fit to the −34.8 ppm slice of the Tl−sodalite data is shown in Figure 4c; the isotropic chemical shift, quadrupolar coupling, and asymmetry parameters derived from this fit are summarized in Table 3. Attempts to fit other slices produced results with much larger errors, making it impossible to distinguish whether the line width is due to a distribution of isotropic chemical shifts or quadrupole coupling parameters, or other factors. Averaging over all these fits results in similar parameters to those of the −34.8 ppm slice; these are also listed in Table 3. Figure 5c shows a simulation of the −33.8 ppm slice of the Ag−sodalite spectrum. A quantitative fit of the silver sodalite data could not be performed because of the distortions of the line shape shown in 5b. These distortions are due to either insufficient rf power to evenly excite the whole powder pattern or to the accidental overlap of lines at this external magnetic field strength. Simulations of several slices were performed, and the average value of the parameters is listed in Table 3.

Another possible explanation for the broad peaks in the spectra could be dipolar effects between the aluminum nuclei in the framework and the heavy metal cations; this is especially possible in the case of the thallium sodalite. Dipolar interactions are usually averaged out by MAS, but thallium has a very large magnetogyric constant, so a 10 kHz spinning speed could be inadequate to compensate for the resulting large dipolar coupling. The MQMAS spectrum for $Tl_6[AlSiO_4]_6$ is clearly broader than that of $Ag_6[AlSiO_4]_6$; the same is true of the 1-D MAS ^{27}Al spectra, presented for comparison in Figure 6. These were obtained at the same frequency as the MQMAS spectra, but a simple one-pulse sequence was used (40 scans with 2 μs pulse width and 1 s recovery time). The Bruker software was used to fit the spectra to one aluminum site, and the resulting quadrupolar parameters are in good agreement with those derived from the multiple quantum experiments (see Table 3). Line broadening of 650 Hz was used to fit the spectrum of $Ag_6[AlSiO_4]_6$; a larger amount (900 Hz) was necessary for $Tl_6[AlSiO_4]_6$. Both spectra show a small peak at 60 ppm that is

TABLE 3: NMR Parameters[a]

		^{27}Al δ_{iso} (ppm)		^{27}Al QCC (MHz)		^{27}Al η	
compound	^{29}Si (ppm)	MAS	MQMAS	MAS	MQMAS	MAS	MQMAS
$Ag_6[AlSiO_4]_6$	−87.0	57.20	57.2 ± 0.5	4.58	4.4 ± 0.5	0.20	<0.3
$Tl_6[AlSiO_4]_6$	−89.9	59.67	60.22 ± 0.03	4.09	4.17 ± 0.02	0.30	0.290 ± 0.004
			59.9 ± 0.5		4.2 ± 0.1		0.2 ± 0.1

[a] δ_{iso} = isotropic chemical shift; QCC = quadrupolar coupling constant; η = asymmetry parameter.

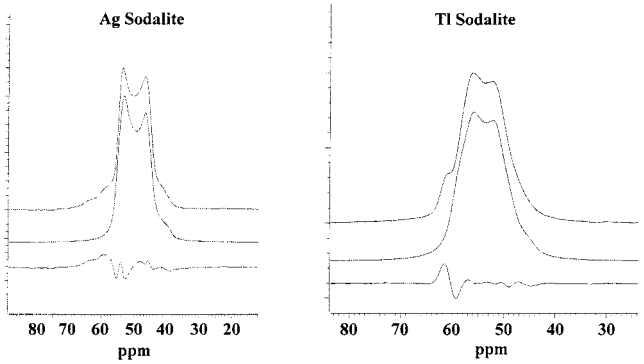

Figure 6. ^{27}Al MAS spectra and fits for $Ag_6[AlSiO_4]_6$ and $Tl_6[AlSiO_4]_6$. Spectra were measured at 130.34 MHz, with the samples spinning at 10 kHz. The top spectrum is the experimental data; the second spectrum is the calculated spectrum based on parameters listed in Table 4, and the difference curve is shown at the bottom.

not affected by quadrupolar effects. This indicates some rehydration of the sodalites has occurred; the hydrated sodalites are cubic and show no quadrupolar shifts or broadening in their ^{27}Al spectra.

^{29}Si MAS experiments were run on both samples using a 4 μs pulse width (90° pulse) and a 5 min recycle delay. A single, somewhat broad peak (400 Hz fwhm) is seen for each sodalite, at −87.0 ppm for $Ag_6[AlSiO_4]_6$ and −89.9 ppm for $Tl_6[AlSiO_4]_6$. This could possibly indicate either dipole coupling or a narrow distribution of Si sites as well, which cannot be easily discerned since the silicon nucleus (spin-1/2) has no quadrupole moment to interact with the several slightly different electric field gradients that are present.

FTIR. IR data was collected on KBr pellets prepared in a glovebox and pressed under vacuum; a Nicolet Magna IR 850 Series II FTIR spectrometer was used. CsI pellets were also prepared to verify that cation exchange with the pellet salt matrix was not a factor in the IR spectra.[18] All the observable IR bands for sodalite are due to the framework; phonon motions of the cations would be found below 400 cm^{-1}, and are therefore out of spectrometer range. On the basis of the crystal structure and space group of this compound, normal-mode analysis indicates there should be 14 IR-active framework modes. Four of these bands, located below 500 cm^{-1}, are calculated to have less than 0.5% the intensity of the strongest band and will not be observable in the spectrum. Two other weak framework modes are found below 400 cm^{-1}. Of the remaining eight bands, three involve asymmetric T−O stretching and are found in the 1000 cm^{-1} region; the band at highest wavenumber is the most intense peak in the spectrum, usually overlapping the other two peaks in this region. Three distinct medium-intensity bands due to symmetric T−O stretching are expected in the 600−700 cm^{-1} region. Two peaks due to O−T−O bending are found in the low-energy region between 400 and 500 cm^{-1}.[19]

The spectra for the two sodalites studied here are shown in Figure 7; the spectrum of the predominantly electrostatic analogue $Na_6[AlSiO_4]_6$ is provided for comparison. The data are summarized in Table 4 and compared to the assignments made in the theoretical study[19] of halosodalites such as $K_8[AlSiO_4]_6Cl_2$. The identity of the framework modes should not be affected by the presence or absence of the halogen anion; this would only perturb the alkali metal ion modes which fall below 400 cm^{-1}.

Results and Discussion

Sodium and Silver Sodalite. The unit cell edge, framework angles, and tilt of the tetrahedra in the sodalite lattice are all interrelated quantities which depend on the same thing—the contents of the sodalite cage. The size of these guest species and their contact with each other and the framework will either expand or contract the unit cell. Because of their simplicity, the differences in the structures of sodalites $Na_6[AlSiO_4]_6$, $Ag_6[AlSiO_4]_6$, and $Tl_6[AlSiO_4]_6$ can be explained in terms of only two varying interactions: metal to oxygen, and metal to metal. The metal-to-framework oxygen bond can theoretically range from predominantly electrostatic to highly covalent. The metal−metal interactions between the ions in each cage are most commonly viewed as repulsive due to the coulomb forces between the positive charges, but it is possible for a bonding force to exist between certain kinds of M^+ ions. The combination of these two effects can result in unexpected structures and phase transitions.

The sodium-containing sodalite $Na_6[AlSiO_4]_6$ has a slight distortion from cubic symmetry at low temperatures. This has been explained as an ordering of Na_3^{3+} triangles from cage to cage into a possibly incommensurate superstructure.[20] Since the center of mass of the three positive ions is different than the center of mass of the negatively charged framework, each cage has a nonzero dipole moment. A superstructure of such dipoles can have the additional result of slightly tweaking the framework itself out of cubic alignment. Fitting of the resulting small superstructure reflections and the peak splitting at high 2θ angles (as well as the multiple ^{27}Al sites seen in MQ-MAS) to an appropriate space group is currently in progress.[7] Above the phase transition at 250 °C, cubic symmetry is achieved due to thermal motion overcoming the ordering of the Na_3^{3+} triangles, which produces a dynamically disordered structure.[21] To compare this compound to the heavy metal exchanged sodalites, high-temperature data (at 400 °C) was analyzed for $Na_6[AlSiO_4]_6$; the resulting geometry is given in Table 2.

From the unit cell size and Na ion locations, it is clear that all the interactions in this material are electrostatic. This ion has a relatively high charge-to-radius ratio, leading to strong Coulombic repulsion between the ions. They are located as far apart as possible within each cage, close to the plane of the six ring windows; the resulting Na−Na distance of 6.112 Å is well above the sum of the radii.[22] The Na−O distance also indicates predominantly electrostatic forces are at work, since it is greater than the sum of the ionic radii. Overall, these ionic interactions result in a very expanded framework, with a unit cell of 9.1603 Å and a small tilt angle of 9.2°.

In the 100 K structure of $Ag_6[AlSiO_4]_6$, the three Ag atoms are also placed very near the center of the six-ring windows of the β-cage. However, the structure has a substantial tilt, $\langle\varphi\rangle$ =

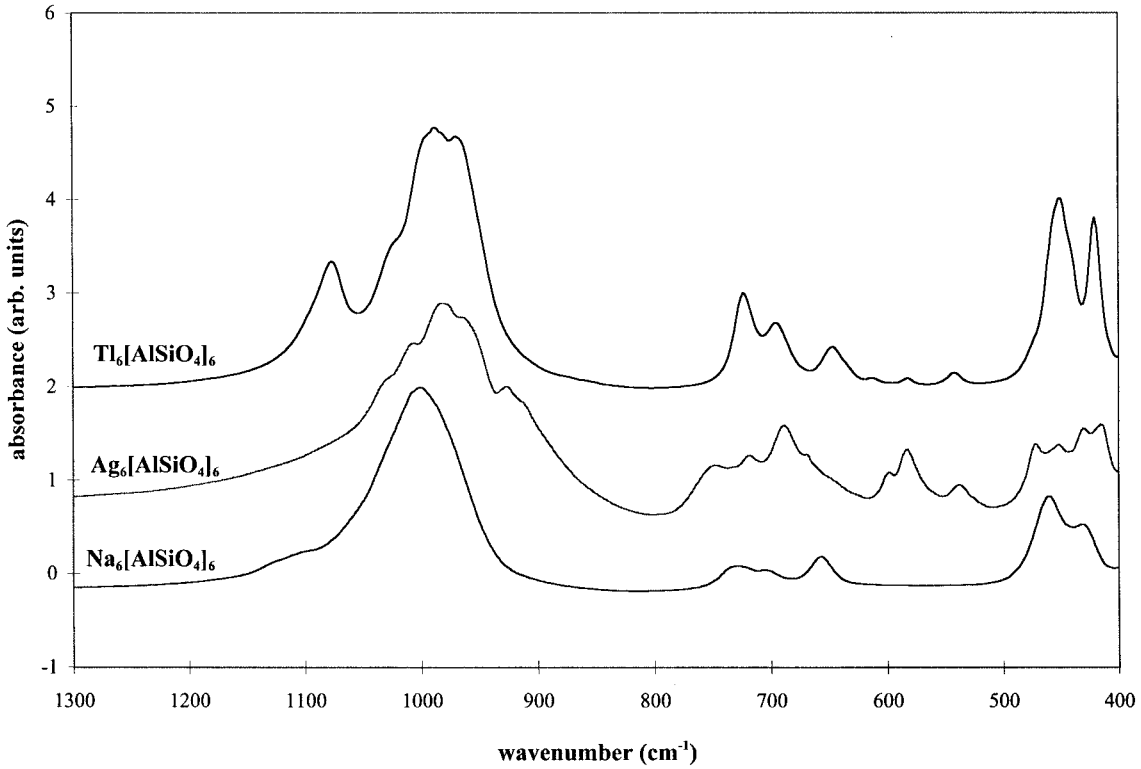

Figure 7. FTIR data for the heavy metal sodalites. For comparison, a spectrum of $Na_6[AlSiO_4]_6$ is also included.

TABLE 4: IR Data for Sodalites

$Ag_6[AlSiO_4]_6$	$Tl_6[AlSiO_4]_6$	$Na_6[AlSiO_4]_6$	assignment
1100 w (s)	1075 s	1100 w (s)	LO phonon mode
1025 w (s)			
1000 vs	980 s	999 vs	TO_4 asym stretch
920 wk (s)	960 s		TO_4 asym stretch
750 med	725 s	727 med	TO_4 sym stretch
715 wk	690 med	704 w	TO_4 sym stretch
680 med	640 med	658 med	TO_4 sym stretch
605 wk	610 w		splitting
585 med	580 w		splitting
540 wk	535 w		splitting
470 med	460 s	461 med	T−O−T bend
455 med			splitting
440 med	425 s	431 med	T−O−T bend
420 med			splitting

15.0°, a unit cell edge of 9.1189 Å, and a reduced Al−O−Si angle of 149.0° compared to 160.5° for a completely expanded framework.[5] Notice that the framework of $Na_6[AlSiO_4]_6$ comes much closer to this theoretical maximum with an Al−O−Si angle of 155.9°, despite having to incorporate smaller ions.

One explanation for this could be the higher charge-to-radius ratio of sodium ions which might result in a larger coulomb repulsion between these three guests, pushing the cage outward to a more expanded state. The polarizability and electronic screening of the nuclear charge of Ag^+ might lower the couloub repulsion between three silver ions, allowing them to be in relative close proximity to each other. A more obvious kind of screening is definitely responsible for the differences between anion-free silver sodalite and its anion-containing analogues. The Al−O−Si angle of the $Ag_6[AlSiO_4]_6$ framework is larger than in the silver halosodalites ($Ag_8[AlSiO_4]_6X_2$, X = Cl, Br, where angles of 140.6° and 141.7° are observed, respectively), despite the fact that the halosodalites contain an extra AgX "salt molecule" in each cage. The anions in the center of the cage result in a screening of the coulomb repulsion between the metal atoms, which allows for a contraction of the structure. In the case of the largest anion (I^-), the screening effect is offset by steric constraints, resulting in a relatively open framework with an Al−O−Si angle of 151.4°.[23]

However, a more crucial factor in the lack of full expansion in $Ag_6[AlSiO_4]_6$ is covalent interactions with the framework, revealed upon looking at the M−O distances. The Ag−O distance is 0.16 Å smaller than the sum of the ionic radii (1.15 Å + 1.35 Å = 2.50 Å), whereas the Na−O distance in the sodium analogue exceeds the sum of ionic radii by 0.19 Å.[22] This is an indication of a degree of covalency between the silver ions and the oxygen of the framework. Also, Behrens reported Ag−L_3 XANES results that suggested covalence was important in $Ag_6[AlSiO_4]_6$.[24] Such a strong covalent tendency can be used to explain the kind of phase transition seen in this sodalite. In a high-temperature study of this compound, it was noted that it undergoes a transition at 678 K from a cubic structure to another cubic structure, with a discontinuity in the thermal expansion. This is evidently driven by the preference of the silver ions for a coordination involving low numbers of strong bonds. As the sodalite is heated, the framework naturally untilts and expands, until a point is reached around 678 K where the silver ions are constrained to be centered exactly in the six-ring window of the fully expanded sodalite, coordinated to a plane of six oxygens at moderate distances of 2.5−2.8 Å. The instability of this position results in a phase transition to another cubic structure in which the Ag^+ ions are again strongly coordinated to only three oxygens.[6c]

This is not the same kind of disorder to order phase transition seen in the sodium analogue. Indeed, neither the silver nor the thallium sodalite has any distortion from cubic symmetry at low temperatures. A plausible reason for this is the lower effective charge on the Tl^+ and Ag^+ ions, caused by their coordination to the framework oxygens and their polarizability. Triangles of such "soft" ions will not form strong dipoles which might interact with those in neighboring cages to force the formation of a superstructure. At the same time cation motion is restricted

in the heavy metal sodalites by the strong bonding to the framework. This prevents incommensurate cation ordering, so there is no resulting distortion of the framework by such aligned dipoles as occurs in the sodium case. Therefore, no phase transition is observed at lower temperatures, and the heavy metal sodalites maintain a pseudo-cubic symmetry due to a locked-in static disorder.

Thallium Sodalite. The dehydrated thallium sodalite has a particularly interesting structure. While it incorporates much larger cations than the sodium or silver analogues, the unit cell is considerably smaller at 8.9653 Å. Part of the explanation is the covalent bonds formed with the oxygens of the framework, as in the silver sodalite. The Tl−O bond length of 2.635 Å is notably shorter than the sum of the radii (1.50 + 1.35 = 2.85 Å), indicating that a large covalent component is present. This does not explain why this compound has a smaller cage size than $Ag_6[AlSiO_4]_6$, however, or why the Tl ions are located well toward the center of the cage instead of close to the plane of the six-ring windows. These discrepancies, along with the unusually short Tl−Tl distances found in the structure, suggest an additional factor is at work.

An intriguing feature of Tl(I) compounds is the presence of its lone pair of 6s electrons. These could play a significant role in $Tl_6[AlSiO_4]_6$. One possibility is that the lone pair on each Tl ion is stereoactive, a condition found in compounds such as Tl_2O, Tl_3ThF_7, Tl_3VO_4, and $TlBePO_4$.[25] Common crystallographic evidence of this includes Tl ions with low coordination numbers, typically three to four short bonds lying all to one side of Tl^+ with very long secondary bonds—and the lone pair—on the other side.[26] This is a good description of the thallium environment in this sodalite; however, stereoactivity is still unlikely. The lone pairs would all be pointing toward the center of the sodalite cage, and since the Tl ions are so close together in this structure, such an electronic distribution would lead to a high-energy coulomb repulsion. Another prospect is that the electron pairs are not stereoactive at all, and are instead localized on their parent atoms in $6s^2$ orbitals with strictly spherical symmetry. Support for this could be inferred from the crystallographic environment of each thallium. The O−Tl−O angles are very near 90°, indicating the Tl−O bonds can be described in terms of oxygen lone pairs in sp^3 orbitals interacting with empty 6p orbitals on thallium. This would necessitate the Tl lone pair being in a purely $6s^2$ orbital. Such simplistic atomic orbital theories are rarely applicable for heavy metals, however, which often utilize higher energy d orbital hybrids for bonding. Also, this does not explain why the Tl sodalite framework is so contracted.

Another possibility is that the lone pairs electrons could be involved in bonding interactions between the three thallium ions in each cage. Formation of a compact Tl_3^{3+} species would help to account for the shrinkage of the sodalite framework. Attractive forces between formally closed-shell (d^{10} or $d^{10}s^2$) ions have been observed and studied in several classes of compounds, particularly gold(I) complexes.[27] It has recently become evident that, in many crystal structures of organothallium compounds, weak attractions between Tl(I) centers seem to determine the mode of molecular aggregation in the solid. Dimeric and polymeric structures are often observed, linked by Tl−Tl bonds.[28]

The nature of these "bonds" has been the topic of some debate. Janiak and Hoffmann did extended Huckel calculations on RTl−TlR dimeric species, concluding that mixing of empty 6p orbitals with the filled 6s orbitals allows a weak covalent bond to form. From these results it was inferred that any Tl−Tl contact within about 0.2 Å of the distances seen in thallium metal (3.4 Å), occurring in the absence of bridging, is suggestive of Tl−Tl bonding.[29] Conversely, Schwerdtfeger noted that extended Huckel calculations are not reliable for estimating molecular properties of heavy element compounds where relativistic effects become increasingly important. His calculations, which involved high-level ab initio theory, including configuration interaction and relativistic effects in the form of relativistic core pseudopotentials, predicted very little covalent bonding between Tl(I) centers.[30] Several other groups have characterized the observed metal−metal linkages as dispersive interactions. Forces of this kind scale with the electron density and polarizability of the atoms and could be significant for thallium.[28,31]

Whatever the nature of the bond, it is clearly strong enough to act as a structure-directing agent. In the literature, several complexes of cyclopentadienes and anionic amides, which have well-established structural chemistry with alkali metal ions, have been exchanged with thallium. This results in solid state structures very different from those of the lithium precursors, usually involving formation of dimers or chains of molecules linked by Tl−Tl interactions.[28] Often such a bond is formed despite the steric hindrance of bulky organic substituents, as in the case of the dimeric pentabenzylcyclopentadienyl thallium (I) complex.[28e] In some cases, the structure of the molecule itself is distorted to facilitate the metal−metal linkage. The tripodal $MeSi[SiMe_2N^-Bu^t(M^+)]_3$ has an adamantoid structure with M = Li, but this is greatly distorted when lithium is exchanged for thallium due to formation of inter- and intramolecular metal−metal interactions.[28b] Common Tl−Tl distances found in such organothallium materials are 3.5−3.8 Å, longer than those in thallium metal, but much shorter than the sum of the van der Waals radii. The Tl−Tl distance of 3.734 Å observed in $Tl_6[AlSiO_4]_6$ is in this range as well. It is therefore reasonable to assume that a weakly bound Tl_3^{3+} cluster is formed. At the same time, the covalent bonds between each thallium and three framework oxygens will pull the framework in, resulting in a smaller unit cell.

Nature of Framework−Cation Interaction. While structural data from X-ray diffraction is somewhat indicative of the electronic distribution in a solid, it is not possible by bond lengths alone to properly characterize atomic interactions. Such characterization can be performed based on the analysis of electron density distributions derived from high-quality single-crystal X-ray diffraction data.[32] However, in the case of disordered systems, diffraction measurements give information only about the time- and space-averaged structure. This is a problem in the case of these anion-free sodalites. Of the four possible cationic sites in the cage, only three are occupied; the framework atoms near the vacant site will have a different electron distribution than those that are perturbed by the presence of a cation. Because these vacancies are randomized in the heavy metal sodalites, their effect is not seen in the averaged structure observed by X-ray diffraction. NMR and IR, on the other hand, are sensitive to local perturbations of a specific nucleus or bond, which will result in peak splitting or shifting. Not only do NMR and IR spectra give information about the local environment, they also offer additional insight into the electronic structure of the moiety in question.

The sensitivity of IR bands to subtle effects on bond force constants are useful in gaining an understanding of localized distortions in the sodalite framework. Small shifts of peaks (±20 cm^{-1}) are expected due to the framework tilting when cations are exchanged for others of a different size. Several investiga-

tions on a number of sodalites have determined that as the Al−O−Si angle increases, the ν_{asym} modes shift in a linear fashion to higher wavenumbers, and the ν_{sym} modes to lower wavenumbers. These relationships have been explained in terms of the changing hybridization of the oxygen atom as the angle varies and the resulting slight changes in T−O bond strength.[33] The experimentally determined relationships for sodalites[21,33] would predict IR bands at 996, 726, 690, and 655 cm^{-1} for $Ag_6[AlSiO_4]_6$ (with its Al−O−Si angle of 149°), and bands at 979, 740, 706, and 667 cm^{-1} for $Tl_6[AlSiO_4]_6$ (with Al−O−Si angle of 139.6°). These are not in agreement with the IR data for these sodalites, indicating another factor is affecting the T−O bond strength besides the hybridization of the oxygen caused by expansion or contraction of the framework.

In addition to these uncorrelated shifts, the infrared data of the $M_6[AlSiO_4]_6$ samples clearly shows the appearance of extra modes in comparison to the spectrum of $Na_6[AlSiO_4]_6$ and the theoretical and experimental data on halosodalites[19] such as $K_8[AlSiO_4]_6Cl_2$ and $Na_8[AlSiO_4]_6Br_2$, all of which can serve as examples of systems in which interactions between cations and the framework are ionic. In particular, the ν_{sym} and δ(OTO) modes of the silver sodalite appear to be split into doublets (any splitting of the ν_{asym} modes at 1000 cm^{-1} would probably be overlapped by the intense original peak, although such splitting is evidenced by the broadening of this mode in comparison to the same one for $Na_6[AlSiO_4]_6$). The extent of this splitting—about 100 cm^{-1} for the ν_{sym} modes—indicates a drastic change in force constant that cannot be explained by the usual factors used to justify smaller shifts of these peaks. The doublets seem to indicate the presence of two "kinds" of T−O bonds: the normal, uncoordinated kind at the accepted wavenumber range, and the metal-coordinated one, weakened (and therefore elongated) by the removal of electron density and therefore shifted to much lower wavenumbers. The stretching force constant would be affected to a greater extent than the bending force constant by lowered electron density, so the large shift of the three "doubles" of the ν_{sym} modes down to 540−605 cm^{-1} compared to the relatively small splitting of the bending modes at 400−500 cm^{-1} is understandable.

On the basis of the fact that there are three cations distributed randomly among the four sites in each cage, a distribution of the two different T−O bonds about each T-site is expected, $O_nT(O\cdots M)_{4-n}$ where $0 \leq n \leq 4$. Statistically, the most likely ratio of normal T−O bonds to elongated T−O···M bonds for one T site is 1:3. [34] This theoretically predominant OT(O···M)$_3$ moiety results in a near-C_{3v} symmetry environment about each framework silicon and aluminum site. Because of the random distribution of the cations, the local effect on the T−O bonds is not seen in the X-ray, and only "average" T−O distances can be determined from diffraction data. However, the perturbation of the T−O bonds is seen in the IR, and the electric field gradient present due to the C_{3v} symmetry is apparent in the NMR data, resulting in a large quadrupolar coupling constant.

The ^{27}Al quadrupolar coupling constant has been linked to the asymmetry of the AlO_4 tetrahedron in many materials.[35] This relationship is somewhat expected, since it is the four oxygen atoms surrounding the aluminum atom that are predominantly responsible for any electric field present at the Al site. Any asymmetry in the distribution of oxygen atoms will result in a field gradient which can interact with the quadrupole moment of the ^{27}Al nucleus. Because of the asymmetry of the local environment of the aluminum sites in these heavy metal sodalites—three elongated metal-coordinated Al−O bonds and one normal bond—a large QCC is expected and is indeed observed. The values seen for silver and thallium sodalite are both above 4 MHz; in predominantly ionic alkali metal halosodalites such as $Na_8[AlSiO_4]_6Br_2$, the corresponding values are all below 1 MHz.[36] A comparison with $Na_6[AlSiO_4]_6$ is not possible because of the slight distortion and lowered symmetry of the framework;[7,14c] this results in multiple Al environments and will affect both chemical shift and QCC.

Large QCC's are also noted in zeolites with acid sites. Catalytically active zeolites (in their protonated form) exhibit the largest ^{27}Al quadrupole coupling constants known so far (11−18 MHz).[37] This results from the formation of a covalent O−H bond at an oxygen site adjacent to the aluminum nucleus being investigated. Koller et al. noted in their theoretical study of acidic zeolites and probe molecules that the removal of electron density from the Al−O bond resulted in a change in bond length of up to 0.2 Å. This produces a very distorted local AlO_4 environment with one very long Al−O bond and the other three slightly shortened; the resulting average of the Al−O bond lengths is in the normal range. A correlation was derived between the calculated QCC and the bond order of the bond between the Al nucleus and the protonated oxygen.[38] By modeling the effects of adding basic probe molecules (such as ammonia or acetonitrile), it was confirmed that factors affecting the strength of the O−H bond have a corresponding effect on the Al−O bond and therefore the QCC.

It is therefore reasonable to assume that the large QCC's seen for the sodalites are predominantly due to the asymmetry of the AlO_4 tetrahedra brought on by the bonding of the heavy metal cations to the framework oxygen atoms. This is a weaker covalent interaction than the O−H bonds in acidic zeolites. Also, it is averaged over three M−O bonds; each heavy metal cation interacts with three of the oxygens in the six-ring window. The three effected Al−O bonds will not be lengthened as drastically as one adjacent to an acid site, so the electric field gradient is smaller, producing a QCC around 4 MHz. The asymmetry parameter values of around 0.3 confirm that the symmetry at the aluminum nucleus is close to axial (C_{3v}), but not quite. This indicates that the location and charge of the cations also play a role in producing the large QCC's at the aluminum sites, but since this effect scales as $1/r^3$, their role is likely smaller than that of the oxygen atoms.

This covalent guest−framework interaction is a likely reason previously derived correlations between NMR or IR data and sodalite structural parameters do not hold for these heavy metal sodalites. For instance, the linear relationships that have been determined between both Al and Si isotropic chemical shifts and structural parameters such as unit cell edge and Al−O−Si angle[39] do not predict the shifts seen for $Ag_6[AlSiO_4]_6$ and $Tl_6[AlSiO_4]_6$. The correlations in the literature were derived from the spectra of alkali metal containing halosodalites, compounds that can be described in terms of primarily electrostatic interactions. A covalent bond between the charge-balancing cation and the framework oxygens will perturb the electron density of bonds and nuclei nearby, and the NMR spectra will be affected accordingly. The NMR signals are in the correct regions for tetrahedrally coordinated, strictly alternating Si and Al sites in an aluminosilicate framework (55 to 70 ppm for ^{27}Al, and −75 to −90 ppm for ^{29}Si), but they vary from the values predicted based on their Al−O−Si angles by 2−5 ppm. This is an indication that the framework cannot be treated as being an isolated system in these heavy metal sodalites.

Another crucial piece of information that can be derived from the NMR is that, in contrast to the expected distribution of

$O_nT(O\cdots M)_{4-n}$ environments, only one kind of aluminum site is present in the heavy metal sodalites. The MQMAS spectra are slightly broadened; this could indicate a distribution of sites, or it might simply be due to dipolar effects. However, the 1-D MAS spectra are quite obviously well-fitted to one site, with parameters in agreement with the MQMAS data. This evidence of one unique aluminum site suggests that the cations have managed to distribute themselves on three of the four possible cation sites in each cage in a manner that allows every aluminum atom to have the same coordination sphere, but does not form a superstructure. The statistically most likely moiety of $OAl(O\cdots M)_3$ would produce an appreciable QCC and would have an asymmetry parameter value of $0 < \eta < 0.3$, in agreement with the values derived from the NMR data.[34] There is the possibility that such an arrangement of the Tl^+ and Ag^+ ions produces some ordering into a cationic superstructure, but that it is not ordered on a long enough scale to produce discernible X-ray peaks.

Conclusion

Structural and spectroscopic data all indicate that there is significant covalency in the interaction between heavy metal charge-balancing cations and the oxygen atoms in the sodalite framework. This results in shrinkage of the unit cell, a large electric field gradient at the aluminum atoms, and the absence of the symmetry-breaking and phase transition characteristics of the sodium sodalite precursor. Further investigation into the electron distribution and the possibility of a cation−oxygen bond will be carried out by implementing maximum entropy method (MEM) calculations on the synchrotron data.

In the thallium sodalite, it is also likely that a weak bonding interaction between Tl ions is present, forming a Tl_3^{3+} cluster in each cage and further shrinking the framework. Additional studies including ^{205}Tl NMR, UV/vis, and far-IR spectroscopy are planned to investigate this cluster. Some interesting fluorescence behavior has been observed in preliminary luminescence studies on this compound which may be related to metal−metal interactions within the cluster.

Acknowledgment. This research was supported by ONR Grant N00014-96-1-0053, NSF Grant DMR-95-20971, and QUEST, an NSF Science and Technology Center for Quantized Electronic Structures (Grant DMR-91-20007). NMR, ICP, and IR studies were done at UCSB Materials Research Laboratory Central Facilities, supported by NSF under Award DMR-96-32716. Studies at the X7B beam line at NSLS, Brookhaven National Laboratory, were supported under Contract AC02-76CH00016 with the U.S. Department of Energy, Office of Basic Energy Sciences. The authors acknowledge Vojislav Srdanov, Nick Blake, and Horia Metiu for informative discussions during the preparation of this paper.

Supporting Information Available: Synchrotron data collection parameters. This material is available free of charge via the Internet at http://pubs.acs.org.

References and Notes

(1) Pauling, L. *Z. Kristallographie* **1930**, *74*, 213−225.

(2) (a) Stein, A.; MacDonald, P. M.; Ozin, G. A.; Stucky, G. D. *J. Phys. Chem.* **1990**, *94*, 6943−6948. (b) Stein, A.; Ozin, G. A.; Stucky, G. D. *J. Am. Chem. Soc*. **1990**, *112*, 904−905.

(3) (a) Blake, N. P.; Srdanov, V. I.; Stucky, G. D.; Metiu, H. *J. Chem. Phys.* **1996**, *104*, 8721−8729. (b) Monnier, A.; Srdanov, V.; Stucky, G.; Metiu, H. *J. Chem. Phys.* **1994**, *100*, 6944−6952. (c) Srdanov, V. I.; Haug, K.; Metiu, H.; Stucky, G. D. *J. Phys. Chem.* **1992**, *96*, 9039−9043. (d) Edwards, P. P.; Woodall, L. J.; Anderson, P. A.; Armstrong, A. R.; Slaski, M. *Chem. Soc. Rev.* **1993**, 305−312. (e) Barrer, R. M.; Cole, J. F. *J. Phys. Chem. Solids* **1968**, *29*, 1755−1758.

(4) (a) Ozin, G. A.; Kuperman, A.; Stein, A. *Angew. Chem.* **1989**, *101*, 373−390. (b) Stucky, G. D.; Macdougall, J. E. *Science* **1990**, *247*, 669−678.

(5) (a) Taylor, D. *Mineral. Mag.* **1972**, *38*, 593−604. (b) Hassan, I.; Grundy, H. D. *Acta Crystallogr.* **1984**, *B40*, 6−13.

(6) (a) Depmeier, W. *Acta Crystallogr.* **1984**, *B40*, 185−191. (b) Depmeier, W. *Z. Kristallographie* **1992**, *199*, 75−89. (c) Behrens, P.; Kempa, P. B.; Assmann, S.; Wiebcke, M.; Felsche, J. *J. Solid State Chem.* **1995**, *115*, 55−65.

(7) Latturner, S. E.; Sachleben, J.; Iversen, B. B.; Srdanov, V. I.; Stucky, G. D. Unpublished results.

(8) Norby, P. *J. Appl. Crystallogr.* **1997**, *30*, 21−30.

(9) Iversen, B. B. Ph.D. Thesis, University of Aarhus, Denmark, 1995.

(10) Willis, B. T. M.; Pryor, A. W. *Thermal Vibrations in Crystallography*; Cambridge University Press: New York, 1974.

(11) Larsson, A. C.; von Dreele, R. B. Program GSAS, LANSCE, MS-H805; Los Alamos National Laboratory.

(12) Lowenstein, W. *Am. Mineral.* **1954**, *39*, 92.

(13) Freude, D.; Haase, J. *NMR: Basic Princ. Prog.* **1994**, *29*, 1−90.

(14) (a) Jelinek, R.; Chmelka, B. F.; Stein, A.; Ozin, G. A. *J. Phys. Chem.* **1992**, *96*, 6744−6752. (b) Engelhardt, G.; Koller, H.; Sieger, P.; Depmeier, W.; Samoson, A. *Solid State Nucl. Magn. Reson.* **1992**, *1*, 127−135. (c) Engelhardt, G.; Sieger, P.; Felsche, J. *Anal. Chim. Acta* **1993**, *283*, 967−985.

(15) (a) Medek, A.; Harwood, J. S.; Frydman, L. *J. Am. Chem. Soc.* **1995**, *117*, 12779−12787. (b) Massiot, D.; Touzo, B.; Trumeau, D.; Coutures, J. P.; Virlet, J.; Florian, P.; Grandinetti, P. J. *Solid State Nucl. Magn. Reson.* **1996**, *6*, 73−83.

(16) (a) Fernandez, C.; Amoureux, J. P. *Chem. Phys. Lett.* **1995**, *242*, 449−454. (b) Rocha, J.; Lourenco, J. P.; Ribeiro, M. F.; Fernandez, C.; Amoureux, J. P. *Zeolites* **1997**, *19*, 156−160. (c) Sarv, P.; Fernandez, C.; Amoureux, J. P.; Keskinen, K. *J. Phys. Chem.* **1996**, *100*, 19223−19226. (d) Baltisberger, J. H.; Xu, Z.; Stebbins, J. F.; Wang, S. H.; Pines, A. *J. Am. Chem. Soc.* **1996**, *118*, 7209−7214.

(17) Grandinetti, P. J. *Program QUADFIT*. Ohio State University.

(18) Flanigen, E. M. In *Zeolite Chemistry and Catalysis*; ACS Monograph Series 171; Rabo, J. A., Ed.; American Chemical Society, Washington, DC, 1976; pp 80−117.

(19) Creighton, J. A.; Deckman, H. W.; Newsam, J. M. *J. Phys. Chem.*. **1994**, *98*, 448−459.

(20) Campbell, B. J.; Iversen, B. B.; Delgado, J. M.; Blake, N. P.; Shannon, S. R.; Latturner, S. E.; Stucky, G. D.; Cheetham, A. K. Unpublished results.

(21) Sieger, P. Ph.D. Thesis, Universität Konstanz, Germany, 1992; p 57.

(22) Shannon, R. D. *Acta Crystallogr. A* **1976**, *A32*, 751−767.

(23) Stein, A.; Meszaros, M.; MacDonald, P. M.; Ozin, G. A. et al. *Adv. Mater.* **1991**, *3*, 306−309.

(24) Behrens, P. *Solid State Commun.* **1992**, *81*, 235−239.

(25) (a) Wallez, G.; Jaulmes, S.; Elfakir, A.; Quarton, M. *J. Solid State Chem.* **1995**, *114*, 123−128. (b) Jouanneaux, A.; Joubert, O.; Fitch, A. N.; Ganne, M. *Mater. Res. Bull.* **1991**, *26*, 973−982. (c) Gaumet, V.; El-Ghozzi, M.; Avignant, D. *Eur. J. Solid State Inorg. Chem.* **1995**, *32*, 893−905.

(26) Wells, A. F. *Structural Inorganic Chemistry*; Oxford University Press: New York, 1990; p 1172.

(27) (a) Beck, J.; Strahle, J. *Angew. Chem., Int. Ed. Engl.* **1995**, *24*, 409. (b) Schmidbaur, H.; Graf, W.; Muller, G. *Angew. Chem., Int. Ed. Engl.* **1988**, *27*, 417. (c) Scherbaum, F.; Grohmann, A.; Muller, G.; Schmidbaur, H. *Angew. Chem., Int. Ed. Engl.* **1988**, *27*, 1544. (d) Vickery, J. C.; Olmstead, M. M.; Fung, E. Y.; Balch, A. L. *Angew. Chem., Int. Ed. Engl.* **1997**, *36*, 1179−1181.

(28) (a) Hellmann, K. W.; Gade, L. H.; Fleischer, R.; Stalke, D. *Chem. Commun.* **1997**, 527−528. (b) Hellmann, K. W.; Gade, L. H.; Scowen, I. J.; McPartlin, M. *Chem. Commun.* **1996**, 2515−2516. (c) Atencio, R.; Barbera, J.; Cativiela, C.; Lahoz, F. J.; Serrano, J. L.; Zurbano, M. M. *J. Am. Chem. Soc.* **1994**, *116*, 11558−11559. (d) Jutzi, P.; Schnittger, J.; Hursthouse, M. B. *Chem. Ber.* **1991**, *124*, 1693−1697. (e) Schumann, H.; Janiak, C.; Pickardt, J.; Borner, U. *Angew. Chem., Int. Ed. Engl.* **1987**, *26*, 789−790.

(29) Janiak, C.; Hoffmann, R. *J. Am. Chem. Soc.* **1990**, *112*, 5924−5946.

(30) Schwerdtfeger, P. *Inorg. Chem.* **1991**, *30*, 1660−1663.

(31) Krebs, B. *Unkonventionelle Wechselwirkungen in der Chemie metallischer Elemente*; VCH: Weinheim, Germany, 1992.

(32) Coppens, P. *X-ray Charge Densities and Chemical Bonding*; Oxford University Press: New York, 1997.

(33) Taylor, D. *Contrib. Mineral. Petrol.* **1975**, *51*, 39.

(34) Sachleben, J.; Clark, T. Ohio State University. Private communication.

(35) (a) Kovalokova, M.; Grobet, P. J. *Solid State Nucl. Magn. Reson.* **1997**, *9*, 107−113. (b) Engelhardt, G.; Veeman, W. *J. Chem. Soc., Chem.*

Comm. **1993**, 622−623. (c) Engelhardt, G.; Koller, H.; Sieger, P.; Depmeier, W.; Samoson, A. *Solid State Nucl. Magn. Reson*. **1992**, *1*, 127−135. (d) Ghose, S.; Tsang, T. *Am. Mineral*. **1973**, *58*, 748−755.

(36) Nielsen, N. C.; Bildsoe, H.; Jakobsen, H. J.; Norby, P. *Zeolites* **1991**, *11*, 622−632.

(37) (a) Ernst, H.; Freude, D.; Wolf, I. *Chem. Phys. Lett*. **1993**, *212*, 588−596. (b) Hunger, M.; Horvath, T.; Engelhardt, G.; Karge, H. G. *Stud. Surf. Sci.* Catal. **1995**, *94*, 756. (c) Grey, C. P.; Vega, A. J. *J. Am. Chem. Soc*. **1995**, *117*, 8232−8242.

(38) Koller, H.; Meijer, E. L.; van Santen, R. A. *Solid State Nucl. Magn. Reson*. **1997**, *9*, 165−175.

(39) (a) Jacobsen, H. S.; Norby, P.; Bildsoe, H.; Jakobsen, H. J. *Zeolites* **1989**, *9*, 491−495. (b) Lippmaa, E.; Samoson, A.; Magi, M. *J. Am. Chem. Soc*. **1986**, *108*, 1730−1735. (c) Radeglia, R.; Engelhardt, G. *Chem. Phys. Lett*. **1985**, *114*, 28−30. (d) Engelhardt, G.; Luger, S.; Buhl, J. C.; Felsche, J. *Zeolites* **1989**, *9*, 182−186. (e) Newsam, J. M. *J. Phys. Chem*. **1989**, *91*, 1259−1262. (f) Engelhardt, G.; Radeglia, R. *Chem. Phys. Lett*. **1984**, *108*, 271−274.